Clock Synchronization Characterization of the Washington DC Metropolitan Area Quantum Network (DC-QNet)

Wayne McKenzie,[1] Anne Marie Richards,[1] Shirali Patel,[1] Thomas Gerrits,[2] T. G. Akin,[3] Steven Peil,[3] Adam Black,[4] David Tulchinsky,[4] Ya-Shian Li-Baboud,[2] Anouar Rahmouni,[2] Yicheng Shi,[2] Ivan A. Burenkov,[5,6] Alan Mink,[7,2] Nijil Lal,[2] Paulina Kuo,[2] Pranish Shrestha,[2] Mheni Merzouki,[2] Alejandro Rodriguez Perez,[8] Eleanya Onuma,[8] Richard Slonaker,[8] Daniel E. Jones,[9] Atiyya A. Davis,[10] Thomas A. Searles,[10] J. D. Whalen,[11] Matthew Diaz,[12] Kate Collins,[13] Qudsia Quraishi,[9] Bruce Crabill,[14] Oliver Slattery,[2] and Abdella Battou[2]

[1)]*Laboratory for Telecommunication Sciences (LTS)*

[2)]*National Institute of Standards and Technology (NIST)*

[3)]*United States Naval Observatory (USNO)*

[4)]*Naval Research Laboratory (NRL)*

[5)]*Joint Quantum Institute and University of Maryland, College Park, MD 20742*

[6)]*National Institute for Standards and Technology (NIST)*

[7)]*Joint Center for Quantum Information and Computer Science*

[8)]*National Aeronautics and Space Administration (NASA)*

[9)]*DEVCOM Army Research Laboratory (ARL)*

[10)]*Dept. of Electrical & Computer Engineering, University of Illinois Chicago*

[11)]*Computational Physics Inc., Springfield, VA 22151, USA*

[12)]*Dept. of Physics, University of Maryland*

[13)]*IREAP, University of Maryland*

[14)]*Mid-Atlantic Crossroads*

(*Electronic mail: thomas.gerrits@nist.gov)

(*Electronic mail: wmckenzie@ltsnet.net)

Distributed protocols relying on quantum interference, event synchronization, network telemetry, timestamping, and precise time-of-flight measurements require high-precision clock and time synchronization. This study describes the design, development, and characterization of two optical time transfer methods between a network of reference clocks at each laboratory node in the Washington Metropolitan Quantum Network Research Consortium (DC-QNet). With optical time transfer using active electronic stabilization, sub-picosecond time deviation (TDEV) was achieved at integration times between 1 s and 10^5 s over 35 km of deployed fiber. Using the White Rabbit-Precision Time Protocol (WR-PTP), we achieved sub-10 picosecond TDEV at integration times ranging from sub-second to over one day. There is potential to improve WR-PTP time transfer using in-situ compensation methods. Measurement methods were developed to understand the impact of environmental and time-of-flight fluctuations on clock synchronization. Path delay gradients, chromatic dispersion, polarization drift, and optical power variations all contributed to clock synchronization instabilities. For protocols requiring the coexistence of quantum and classical communications, we deployed WR-PTP in a bi-directional configuration using 1270 nm and 1290 nm wavelengths over 64 km. The results from this study will inform future advancements in the development of metropolitan-scale, telecommunications-compatible clock synchronization networks for enabling near-term experimental research in quantum networking protocols.

I. INTRODUCTION

High-precision time and frequency synchronization enables fundamental quantum networking capabilities from measuring the indistinguishability[1] of sources to entanglement distribution[2–4] and swapping[5–7]. Clock network design considerations for quantum networking research include the ability to integrate into existing telecommunications infrastructure, co-propagation of quantum and classical signals[8–11], scalability, resilience, and security. As a single photon pulse duration can vary from several nanoseconds to hundreds of femtoseconds for ultrashort pulsed lasers, our initial goal is to achieve time synchronization at sub-10 picosecond time deviation (TDEV) over long-distance deployed fibers to support the near-term development of protocols relying on quantum interference[12,13].

A quantum network includes both quantum and clas-

sical signals, possibly coexisting on the same channel, to distribute entanglement between nodes. The benefits of quantum networks range from theoretically secure distribution of keys (Quantum Key Distribution[14]), to distributed quantum sensing[15] and computing[16], to secure clock synchronization[17,18]. Many groups are currently developing metropolitan scale quantum networks[19–23], including DC-QNet. This paper will focus on the deployment and characterization of high precision time synchronization, one of the fundamental capabilities of quantum networking, across DC-QNet.

A. Quantum Networking Applications

Quantum state distribution requiring quantum interference (such as teleportation and swapping protocols) relies on the
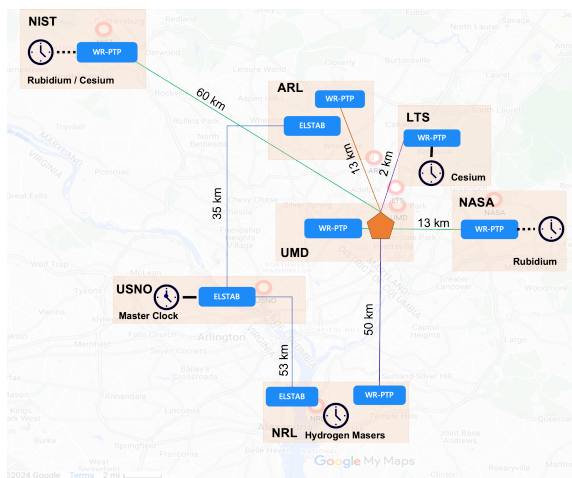
FIG. 1. The DC-QNet is comprised of the National Institute of Standards and Technology (NIST), DEVCOM Army Research Laboratory (ARL), National Aeronautic and Space Administration (NASA), Laboratory for Telecommunication Sciences (LTS), United States Naval Observatory (USNO), and Naval Research Lab (NRL). The DC-QNet includes a network of atomic clocks, where USNO operates the Master Clock ensemble[31,32].

FIG. 2. Frequency stability of clock and OTWTFT models available in the DC-QNet testbed.

near-simultaneous arrival of single photons at the detection plane of remote nodes separated by deployed fiber. The accurate measurement and control of qubit states require the clocks to be precisely synchronized and require the ability to accurately estimate and compensate for variations in the path delay of the fiber. One such protocol is quantum position verification, which protects location-based authentication from undetected interception by adversaries based on the no-cloning property[24–26]. The coexistence of both quantum signals and classical time transfer is necessary to improve path delay estimation, enable phase stabilization for qubit transfer, and improve the scalability of quantum networks by reducing the number of fibers required for communications. Quantum channels tend to be lossy, and experiments are usually on the order of hours to days; therefore, the ability to maintain synchronization precision over both sub-second and longer observation intervals is needed. Classical time and frequency transfer over optical fiber has been demonstrated to achieve the stability requirements[22,27–30] needed for quantum networks.

II. CLOCK SYNCHRONIZATION ARCHITECTURE

As an emerging testbed to advance research in quantum network metrology and protocols, the Washington Metropolitan Quantum Network Research Consortium (DC-QNet) is composed of six agencies in the Washington D.C. area with fiber links currently ranging from four to over 60 kilometers (Fig.1). The initial goal of DC-QNet is to achieve readily scalable sub-10 ps time stability with less than 10^{-11} time deviation (TDEV) to enable the distribution of entangled photons among distant nodes and to provide a suite of meas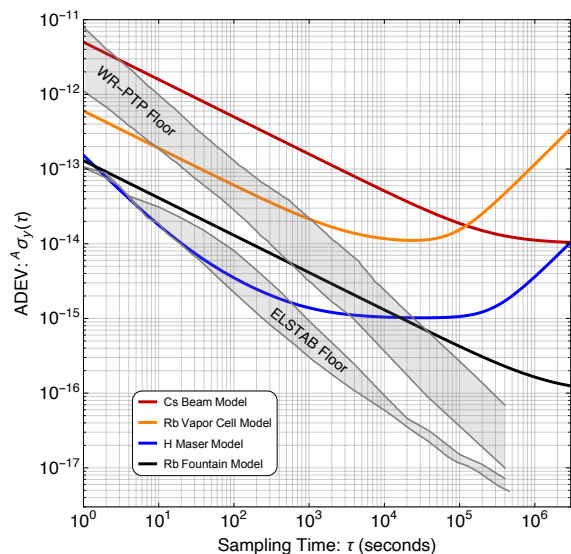urement and control tools needed for metropolitan-scale quantum network research. In this work, the DC-QNet integrated and characterized two optical two-way time-frequency transfer (OTWTFT) methods, each with their benefits and limitations.

A. White Rabbit Precision Time Protocol

The White Rabbit – Precision Time Protocol (WR-PTP), which is now part of the Institute of Electrical and Electronics Engineers (IEEE) 1588-2019 standard as the High-Accuracy Precision Time Protocol (HA-PTP) Profile[33], has been employed in various quantum network testbeds ranging from laboratory to metropolitan-scales[8,20,34,35]. WR-PTP is a classical protocol developed at the European Organization for Nuclear Research (CERN)[36]. WR-PTP uses highly precise round-trip delay measurements with calibrated asymmetry and fixed delay values to achieve sub-nanosecond synchronization precision. WR-PTP has been implemented in open-source hardware and software such as the White Rabbit Switch (WRS)[37].

A two-level cascaded architecture was established with one WRS grandmaster (GM) and one boundary clock (BC) located at NIST in Gaithersburg, MD (Fig.3). Another BC is located 64 km (as measured by Optical Time Domain Reflectometry (OTDR)) away at LTS in College Park, MD. The total round-trip between the two clocks at NIST was 128 km[35]. The implementation of bi-directional WR-PTP time transfer, which economizes the use of deployed fibers, requires the use of two different wavelengths in order to distinguish the transmit signals between the transmitter and the receiver. For dense wavelength division multiplexing (DWDM) channels, circulators and filters were required to reduce the back reflection and to separate the transmit and receive wavelengths within the bi-directional path which can add loss and degrade measurements.

A star topology using duplex fibers has also been established to synchronize multiple nodes to a Cesium clock at LTS and to reduce loss. To design and integrate a time transfer signal that can co-propagate with quantum signals in the low-loss C-Band, we implemented and characterized a bi-directional synchronization architecture[10] using 1270 nm and 1290 nm transceivers.

B. Electronically Stabilized Fiber-Optic Time and Frequency Distribution

An electronically stabilized (ELSTAB) fiber optic time and frequency distribution system is being established in a star topology emanating from the United States Naval Observatory (USNO) Master Clock[31,32], which is based on a highly stable atomic clock ensemble traceable to UTC. ELSTAB applies variable electronic delay lines to compensate for link propagation delay fluctuations[38].

There have been great strides in phase noise compensation of time and frequency transfer over fiber links[38–42]. USNO employs the PIKTime OSTT[38] system as a commercial solution to electronically stabilized fiber-optic time and frequency distribution. This system uses a Local module to transfer a stable RF (usually 10 MHz) and 1 pulse-per-second (PPS) signals to a Remote module at a distant location. The Local module uses a forward-direction variable delay line to correct the fiber phase noise related to environmentally induced variations in fiber length and index of refraction. An intensity-modulated 1549.3 nm laser carries the RF through a circulator to the optical port of the Local module. Receipt of the signal occurs at the far end of the fiber using the Remote module, where the optical information is converted back to an electrical signal. The electrical signal is split, distributing to the end-user and redirecting back to the Local module using a second intensity-modulated 1548.5 nm laser, where a comparison of phase against the input RF generates an error signal for phase noise compensation. The returned RF and PPS signals can be accessed at the Local module. A correction is applied to the phase of the returned RF and PPS signals to cancel the fiber noise from the round-trip, and these signals can be used as a diagnostic of the ELSTAB link. The Remote module has RF and 1 PPS outputs, and can generally achieve a fractional instability of 10^{-13} at one second, which integrates as white phase noise ($1/\tau$).

III. OTWTFT STABILITY CHARACTERIZATION METHODS AND RESULTS

A. White Rabbit Precision Time Protocol (WR-PTP)

A time-correlated single photon counting (TCSPC) module, was used to measure the clock differences at NIST. The constant fraction discriminator's input bandwidth is 4 GHz and the time variance of the instrument response function is below 1 ps at 10^{-6} s up to 1 s integration times. For the loopback measurements taken at LTS, the TCSPC module's timing
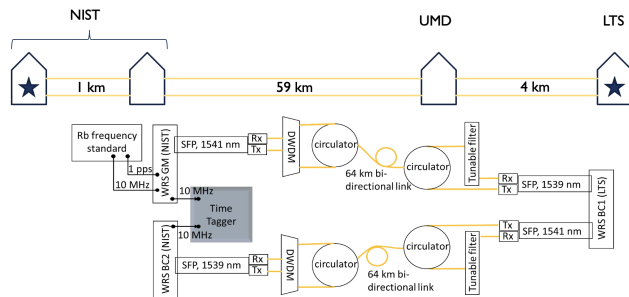

FIG. 3. The NIST WRS GM clock was synchronized to a Rubidium reference. The clock was then distributed to the first boundary clock (BC1) over a 64 km bi-directional fiber. Finally, time is distributed to a final boundary clock (BC2) over a separate 64 km link. A time tagger is used to compared 10 MHz signals from the first and last clocks.
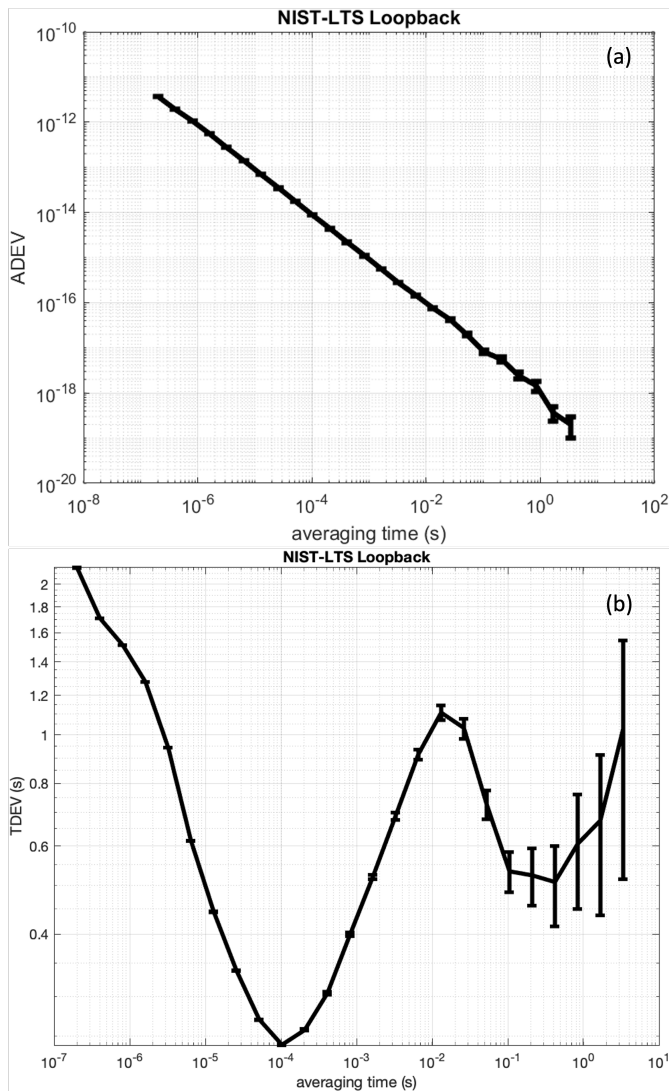

FIG. 4. Sub-second frequency (a) and time (b) stability for the NIST-LTS 128 km loopback topology.
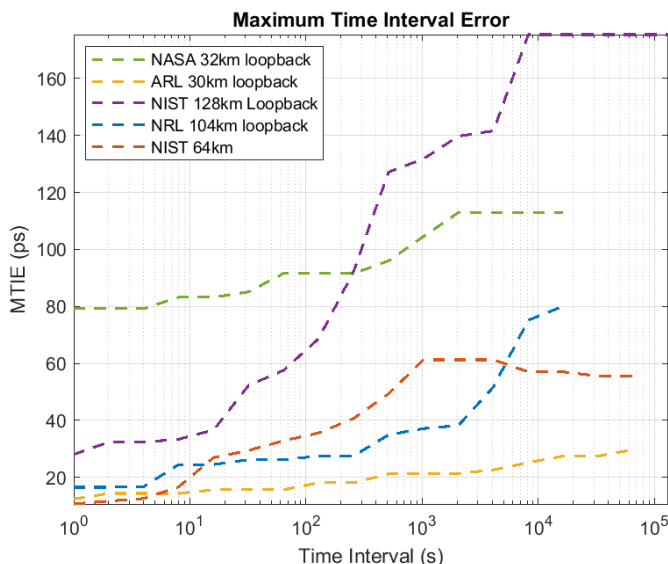
FIG. 5. Maximum Time Interval Error (MTIE) in picoseconds for WR-PTP deployments across five DC-QNet agencies. The clock errors for ARL, NASA and NRL were measured at LTS. The clock errors for the NIST-LTS link were measured at NIST.

jitter was below 2 ps RMS between channels. The 1 Hz round-trip and one-way path delays were provided by the WR monitoring software. The monitoring software was customized to track the small form-factor pluggable (SFP) module receive power and temperature.The air temperature data was acquired from the Open Weather API[43]. The peak-to-peak phase difference between the GM and BC2 was less than 200 ps after subtracting the initial (<1 ns) offset between the two clocks. The Maximum Time Interval Error (MTIE) was used to assess the peak-to-peak time error between the GM and BC2 (Fig.5). At observation intervals ≤ 10 s, the time error was < 25 ps at 1 Hz synchronization rate. The Allan Deviation (ADEV) was used to evaluate the fractional frequency stability (Fig.4 (a),6). The TDEV was below 10 ps, where the noise floor for the most quiet links dipped below 1 ps (Fig. 6(b)). The ADEV between 10^{-6} s and 1 s averaging times were below 10^{-11}. Time transfer over links with the greatest proportions of aerial fibers experience the most frequency and time instabilities. Evidence of this can be seen in the polarization drift as well (Sec. IV D).

B. Electronically Stabilized Time and Frequency Distribution (ELSTAB)

At present, there are two opportunities to characterize the performance of the ELSTAB method by means of the connections shared with USNO. A 10 MHz signal referenced to the USNO Master Clock is transmitted using the PIKTime OSTT system on the link shared by USNO and NRL, as well as on the link shared with USNO and ARL. A Symmetricom 5120A records the relative phase between the reference input and the outputs from the PIKTime systems.
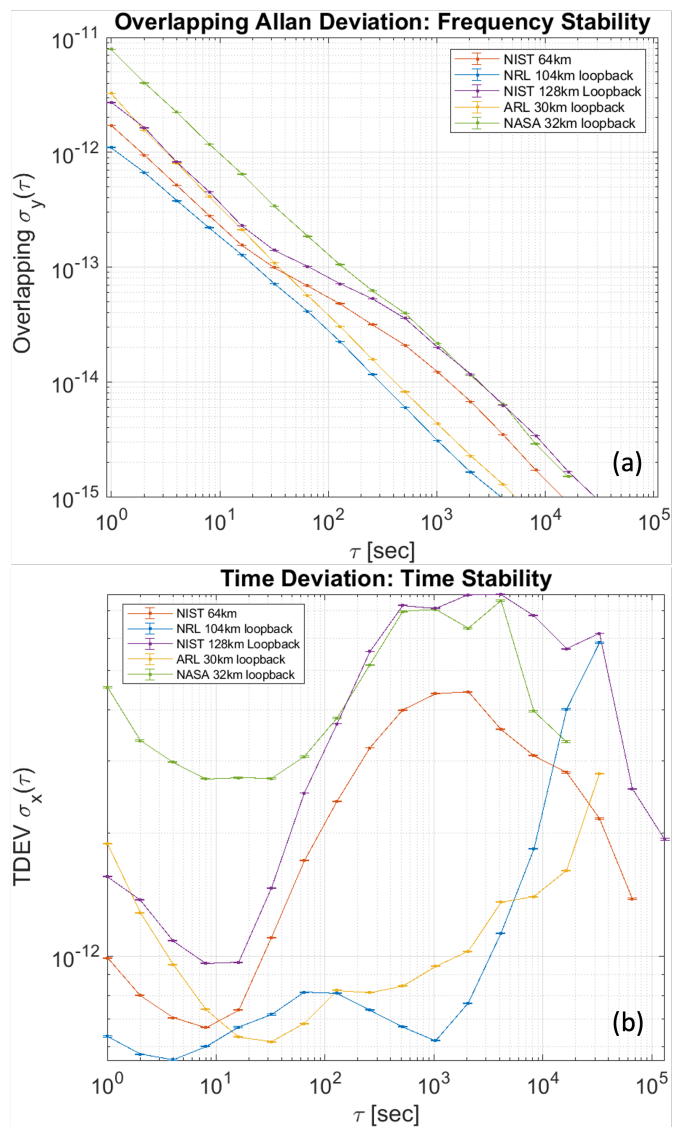

FIG. 6. (a) Overlapping Allan Deviation and (b) Time Deviation for 128 km loopback topology and 64 km star topology.

The link between USNO and NRL has been operating a PIKTime OSTT-2 for several years. In order to maintain continuous operation of this link, we are limited in non-invasive measurements to evaluate the PIKTime system. Our best assessment of its performance is determined by comparing the radio frequency (RF) return against the RF input. Fig. 7 (a) shows several months worth of phase difference between the two signals. Throughout the entire period of data collection, the phase difference did not exceed 10 ps. The ~ 12 hour break in data on 5 September was an undetected, temporary drop in the local data collection. Nonetheless, the PIKTime maintained uninterrupted operation. However, this represents an "in-loop" measurement of the performance. Local access of the Remote output is needed to properly determine the performance of the Remote output.

We can test the out-of-loop performance of the ELSTAB method using a loopback established on a pair of fibers con-
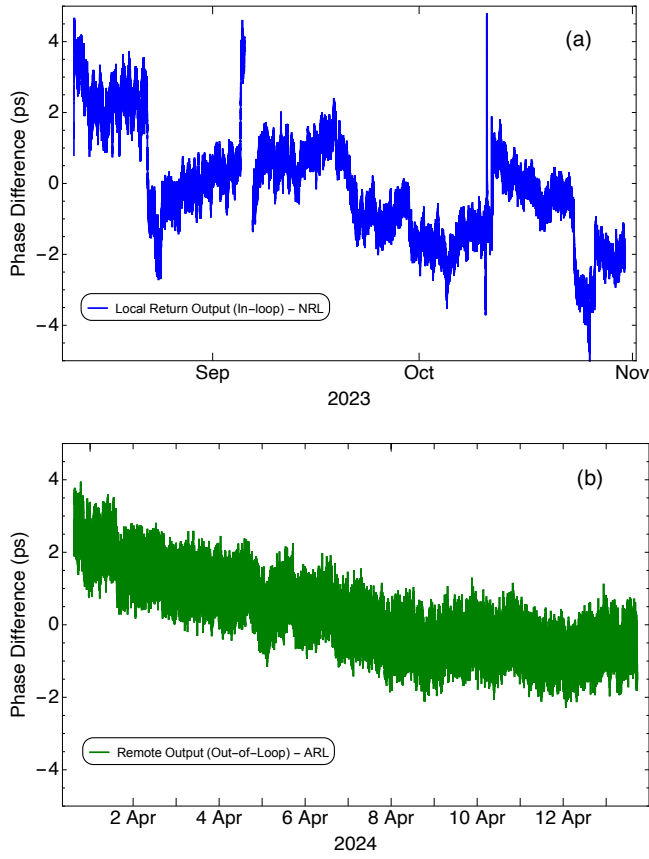
FIG. 7. Phase difference plots between a 10 MHz signal transmitted via PIKTime on a fiber link and the reference for that transmission. (a) The transmission is on the USNO-NRL link. Due to operation constraints, the measurement is made using the "Return" output of the PIKTime Local module. (b) The transmission is on the USNO-ARL link. The loop-back installed on this link allows for direct measurement of the reference versus the output of the PIKTime Remote module.

necting USNO and ARL. With the Local and Remote modules in the same space, a measurement can be performed comparing the Remote output against the input on a ~ 68 km (round trip) metropolitan link. Fig. 7 (b) shows nearly two weeks of phase difference between the Remote output and the input 10 MHz. The phase difference between the two signals does not exceed 10 ps, which is consistent with the performance of the in-loop ELSTAB measurement on USNO-NRL link.

Fig. 8 (a) displays the ADEV for the two measurements described in this subsection. The Remote output on the USNO-ARL link performs as well as the Local return output on the USNO-NRL link for averaging times less than 10 s. For longer averaging times, the Remote output appears to accumulate some additional noise not measured in the Local return output. Without access to the internal components of the Local or Remote modules, we can only speculate on the source of the noise (e.g. competition from multiple reflections at poor splices or connections, or electronic noise in the Remote module that is external to the interferometer path). Fig. 8 (b) shows the corresponding TDEV for the two measurements. Both
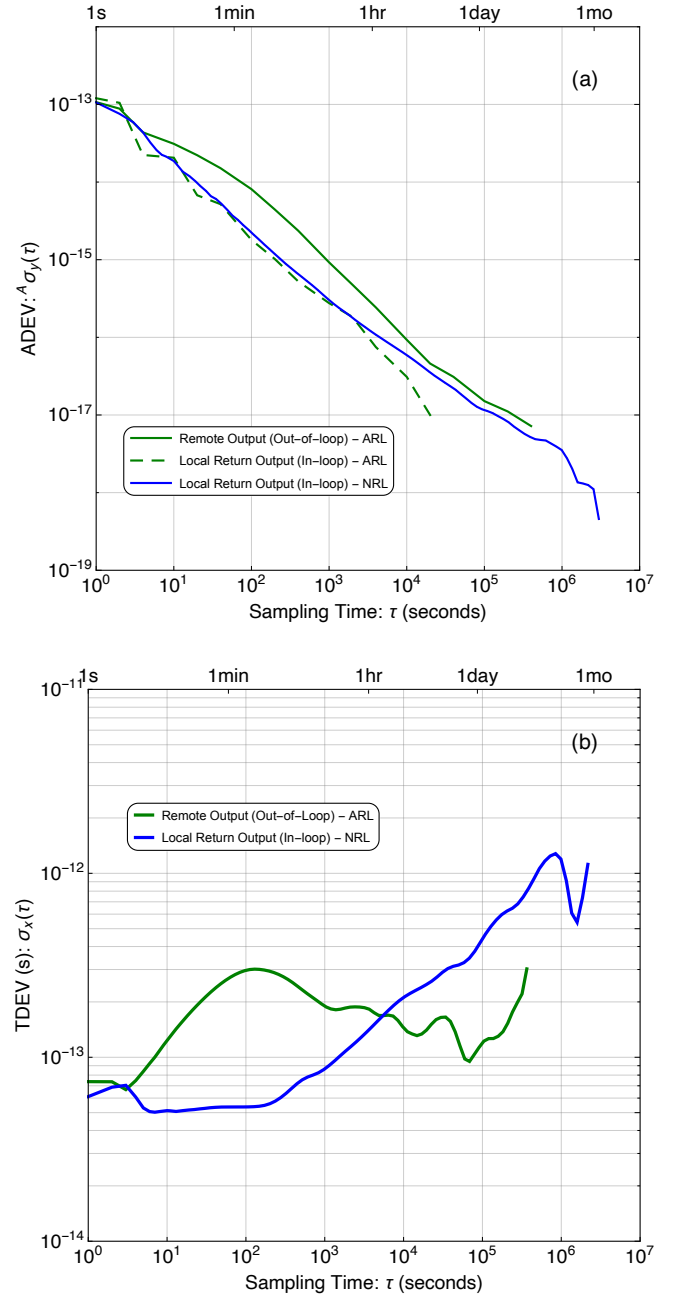

FIG. 8. (a) ADEV for links between USNO and the two agencies connected: NRL (Blue) and ARL (Green). (b) TDEV of the same links.

measurements meet the stability requirements anticipated for most protocols relying on quantum interference.

IV. CLOCK NETWORK CHARACTERIZATION AND RESULTS

Understanding and addressing the challenges of deploying a synchronized network of clocks for quantum network research requires measurement methods beyond typical optical

time transfer characterization where requirements may be several orders of magnitude less stringent. Quantifying and understanding the sources of variations in clock and time transfer error includes both the dominant factors such an environmental changes leading to fluctuations in time-of-flight, but also other factors such as polarization and optical power. Furthermore, achieving co-propagation of quantum and classical channels requires measurement of the noise caused by Raman scattering induced by the classical channel and crosstalk between ports in deployed telecommunications components.

A. Uncompensated Path Delay Measurement

A direct measurement of time-dependent path delay was performed using optical modulation techniques on both the NRL-LTS (52 km) and USNO-ARL (35 km) fiber links. In these measurements, a continuous wave (CW) C-band laser is intensity-modulated at an RF frequency f_{mod} using an electro-optic intensity modulator (IM). The bias phase of the IM is actively stabilized using low-frequency feedback to eliminate slow temperature-driven variation of the operating point of the IM. The modulated light propagates through the dark fiber link and is looped back to its origin on a separate fiber strand. The return signal is detected on a photodiode and measured on a lock-in amplifier with reference frequency f_{mod} derived from the same signal generator that synthesizes the IM RF input. The variation in phase $\Delta\phi$ of the return-signal modulation relative to the synthesizer phase provides a measurement of the variation in group delay $\Delta\tau$ of the total loopback optical link according to $\Delta\tau = \frac{\Delta\phi}{2\pi f_{\mathrm{mod}}}$. This method provides a measurement of optical path delay that is independent of the clock distribution architecture and provides high-bandwidth data in the frequency range from DC to MHz.

In the NRL-LTS uncompensated path delay measurement (Fig. 9), the laser source is a Gooch and Housego AA1406 DFB laser at 1547.3 nm. Modulation is provided by an EOSpace AZ-CK5 IM driven with $f_{\mathrm{mod}} = 100$ MHz, and IM bias stabilization is provided by a Pharad MBC-DF-DM modulator bias controller. The loopback mean path delay is approximately 0.5 ms as measured separately through a time delay of 100 ns optical pulses. As in Fig. 11, the outside air temperature is plotted and a strong correlation is evident between path delay and temperature variation. However, a much smaller path delay amplitude is observed, as is a time delay of roughly 3 hours in the response of fiber path delay to temperature changes. These differences presumably are due to the fact that much of the fiber in the measured connection is buried underground. Low-frequency peaks at 0.36 mHz and 1.6 mHz are observed in the power spectrum. The origin of these features is unknown but could be due to the cycle time of air conditioning in spaces along the fiber path causing high-frequency vibrations and low-frequency temperature variations[44].

The time-dependent path delay of the USNO-ARL fiber link was characterized using a loop-back on the pair of fibers connecting the two agencies. Commercial products are used to perform an optical modulation technique to transmit RF fre-
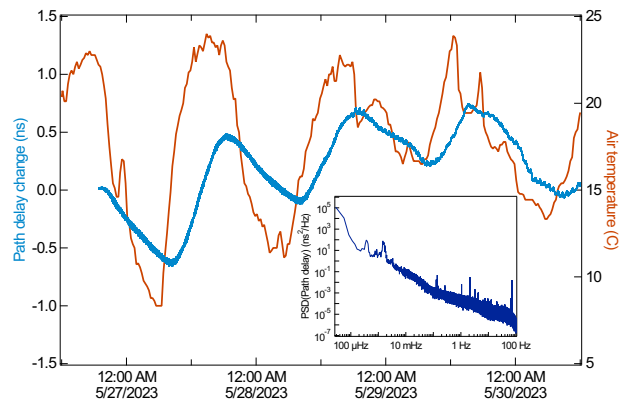

FIG. 9. Plot of uncompensated round-trip path delay between NRL and LTS (see Fig.1) over a four-day period (blue) and temperature measured at the College Park, MD weather station (orange). Inset: power spectral density (PSD) of the path delay time trace.
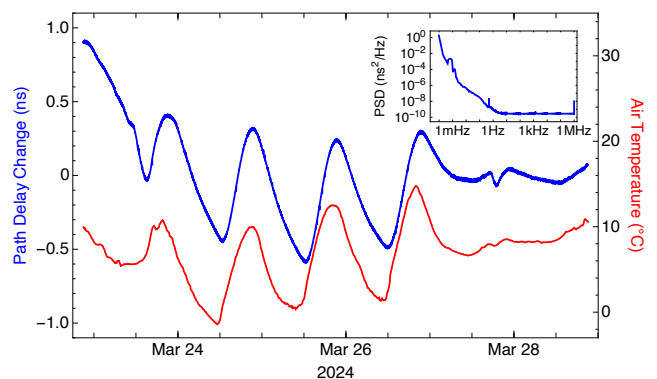

FIG. 10. Plot of uncompensated round-trip path delay between USNO and ARL over a six day period (blue) and temperature measured at a weather station near ARL (red). Inset: power spectral density of the path delay time trace.

quencies over fiber. A pair of Linear Photonics DiLink modules transmit and receive a 10 MHz signal referenced to the USNO Master Clock. A Symmetricom 5120A records the relative phase between the reference for the transmitter module and the output of the receiver module. Fig. 10 shows the change in phase record over a six day period. The mean path delay of 338 μs was determined from an independent, time-interval measurement of a 1PPS signal transmitted on the link. Similar to Figs. 9 and 11, there is a strong correlation to air temperature. As in Fig. 9, the ~ 3 hour lag between delay and temperature change suggests that most of the fiber is buried underground.

B. WR-PTP One-Way Path Delay Estimates

Figure 11 shows the NIST-LTS path delay. The path delay changed by approximately 40 ns peak-to-peak over five days, while the ambient outside temperature varied by about 15°C.
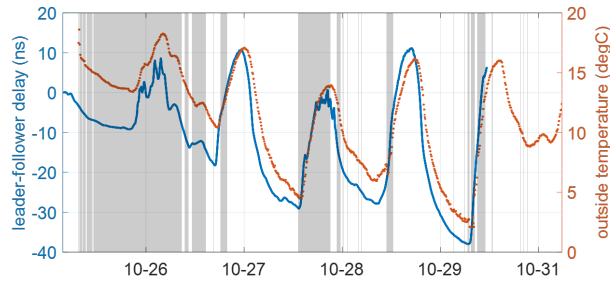
FIG. 11. Plot of path delay over five days between BC1 and BC2 (see Fig.3) and temperature measured at the NIST campus. There is a strong correlation between path delay and temperature variation. The gray boxes depict periods of time with cloud cover.
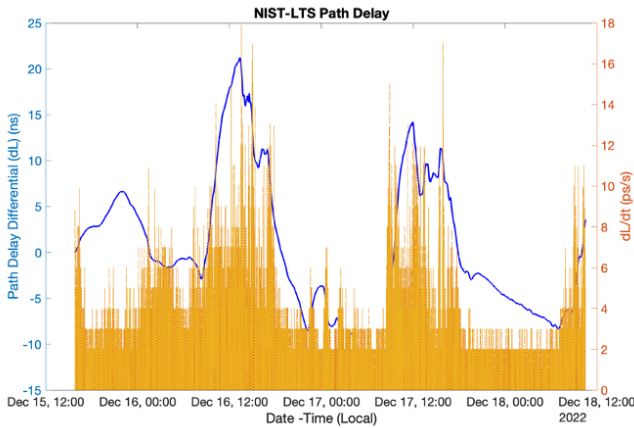

FIG. 13. Variation of SFP wavelength when placed in an incubator at controlled temperatures taken over deployed fiber.

FIG. 12. Plot of one way path delay (blue) and rate of change (orange) for the 64 km aerial link between LTS and NIST.

FIG. 14. Difference between path delay of two parallel fibers in the same fiber bundle.

Shaded regions represent non-clear, i.e. some form of sky coverage, while white regions represent clear skies. Fig. 12 shows the path delay rate of change, $\frac{\Delta L}{\Delta t}$, for aerial fibers. The path delay was measured at the WRS BC using 1539.77 nm SFP transceivers. For the NRL-LTS link, the mean one-way path delay is approximately 0.25 ms. The average path delay rate of change is 0.2 ps/s and the maximum path delay rate of change is 3.5 ps/s. In contrast, the NIST-LTS link had an average path delay rate of change of 1.3 ps/s, and a maximum path delay rate of change of 17.9 ps/s. The path delay gradients coincided with the temperature variations, where temperature is the main source of transit time fluctuations over the NIST-LTS link. The mean one-way path delay is approximately 0.32 ms.

WR-PTP can also be used to measure the fiber link delay for compensating the time of arrival of quantum and classical messages in quantum-augmented network protocols. The one-way path delay measurements from BC1 and BC2 were time aligned and compared, with the initial bias removed from both sets of measurements. The two parallel fibers take the same nominal path and are generally affected by the same changes in delay down to 100s of picoseconds. For adjacent fibers, WR-PTP can also be employed as a probe signal. The result can be improved by reducing the path delay normalization
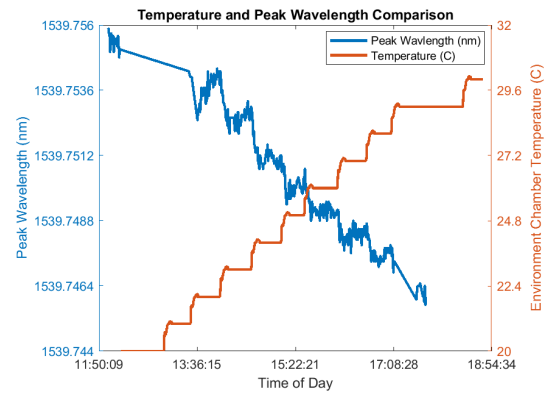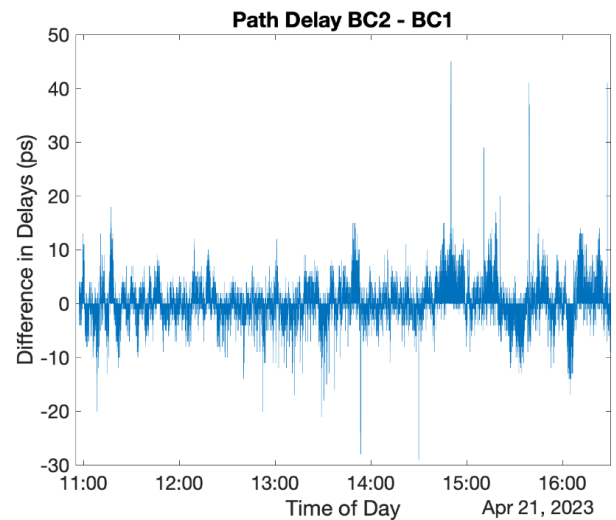
window. Fig. 14 shows the BC2 and BC1 one-way path delay difference with a normalization window of less than 10 s.

C. Chromatic Dispersion

For bi-directional WR-PTP time transfer, two separate wavelengths are used. The SFP laser sources were measured with a spectrometer in the laboratory overnight for both coarse WDM (CWDM) and dense WDM (DWDM) SFPs at ambient room temperature that remained within 2 °C (Fig.13, top plot). The SFP laser varied within 10 pm, the uncertainty of the spectrometer measurements. In the deployed links, the DWDM channels 45 (1541.35 nm) and 47 (1539.77 nm) are used. The 1.6 nm separation results in a constant path delay offset. In addition, there are temperature-dependent wavelength fluctuations. We used an optical spectrum analyzer (OSA) located at LTS to study the characteristics of the fluctuations of the emitted lasers from NIST over the deployed
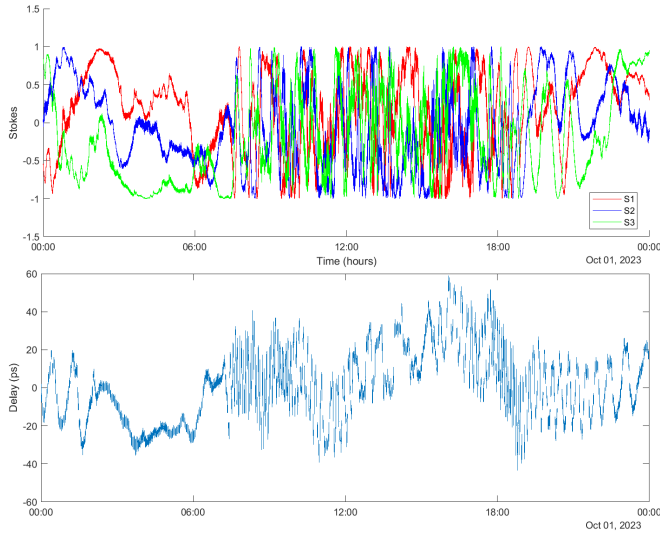
FIG. 15. (Top) Stokes vector variation over the course of 24 hours on the aerial LTS-NIST link. (Bottom) Clock delay variations are measured in a loopback setup. Both plots show similar diurnal variations, with less instability during the night.

fiber (Fig.13). The GM and BC WR switches were placed in an environmental chamber with 0.1 °C uncertainty. The filters and circulators remained in ambient laboratory temperature to understand the effect of device temperature variation on the time error given changes in the fiber temperature. The controlled temperature range was between 20 °C and 30 °C, which corresponded to common temperature variations in the laboratory. Subsequent experiments varied the temperature at a rate of 1 °C every 30 minutes, where an inverse relationship between the peak wavelength and the incubator temperature was observed. The total observed wavelength difference was approximately 10 pm to 15 pm given a 10 °C change in the incubator temperature.

D. Polarization Stability

The polarization stability of the NIST-LTS link was characterized while simultaneously running the WR-PTP protocol. A variable coupler was used to take a portion of the WR-PTP signals, with minimal power loss, to simultaneously measure the polarization state with a polarimeter and to maintain lock between the WR nodes to measure the clock delay. Fig. 15 shows the Stokes parameters and clock delay over 3 days for one of the fibers. Polarization drift was measured on two parallel fiber strands as part of a duplex link. One fiber had a slower polarization drift than the other. There is a clear difference in variations between night and day, in both clock delay and polarization drift. This is largely due to fiber stretching and bending as a result of aerial fiber on the link.

The polarization stability of the ARL-LTS link was also measured. A loopback was placed at LTS, and a polarimeter was used at ARL to characterize the polarization drift of a signal over the 30 km round-trip length of the ARL-LTS link
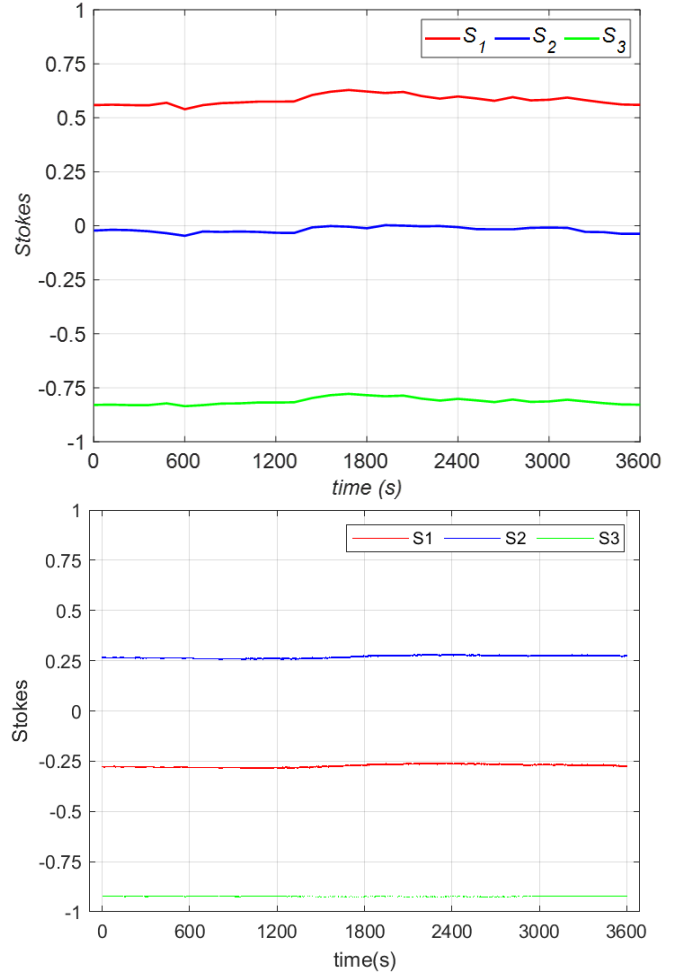

FIG. 16. (Top) Polarization variation of a 30 km loop-back link between ARL and LTS over 1 hour from 12:00 PM -1:00 PM. The average temperature was ~ 7°C. The fiber is buried, resulting in virtually no polarization variation. (Bottom) Similar polarization measurement over underground fiber between LTS and UMD, approximately 3.5 km. This measurement was done from 12:00 PM-1:00 PM on a different day.

(15 km one-way). The Stokes parameters are shown in Fig. 16. The measurement was performed for one hour from 12:00 PM -1:00 PM, local time, i.e. when significant disturbances would be expected for an aerial fiber (as seen in Fig. 15) due to temperature and other environmental factors. However, the polarization remains virtually unchanged over the hour-long period for the buried fiber.

E. Optical Power

Variations around 5 μW as measured using a power meter were observed over the NIST-LTS and NASA-UMD deployed links. To understand the impact of optical power on the clock delay, a controlled experiment with a variable attenuator between the outgoing link over the deployed fiber
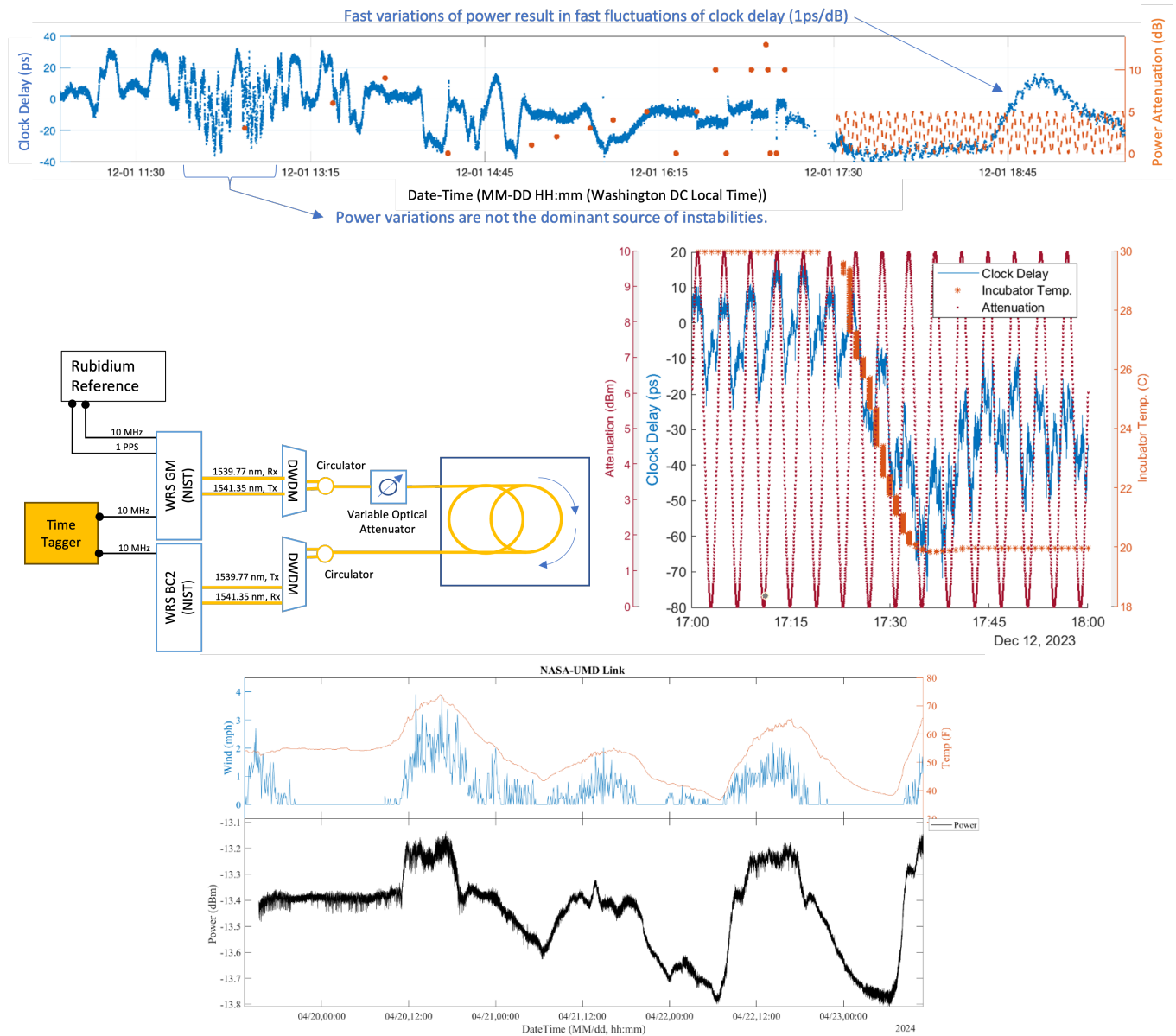
FIG. 17. (Top) Clock delay measurement while varying power attenuation on one side of the link. (Middle-left) Schematic for measuring the temperature, power attenuation, and clock delay simultaneously in the lab. Spools of fiber are placed in a temperature-controlled oven to vary temperature in a controlled manner. (Middle-right) Temperature variation and Power attenuation together cause large dips in clock delay as well as periodic variations. These patterns can be seen in deployed fiber data on the Top plot from 5:30 PM -8:00 PM, local time. (Bottom) An example plot showing the variation of optical power over the primarily aerial NASA-UMD link.

was conducted. The optical power variation was initially confounded by air temperature changes in the link. Once the outdoor temperature stabilized to within 1 °C over several hours and the path delay was relatively stable, a 1 ps change in clock delay per 1 dB of attenuation was observed (Fig. 17 (top)). To disaggregate the impact of air temperature and optical power variations, a subsequent experiment (Fig. 17 (middle)) with 62 km of fiber spools between the GM and BC1 were placed in an incubator at a constant temperature (30 °C) with optical power attenuation cycling between 0 and 10 dB, which induced clock errors on the order of ±20 ps. The experiment

was followed by a 10 °C drop in the incubator temperature when clock delay differences on the order of 100 ps were observed. The results, Fig. 17 (bottom), confirm the air temperature variations, and subsequent effects on path delay gradients, is the dominant factor contributing to clock delay errors.

F. Noise Characterization

A crucial step to achieving coexistence is to understand the noise profile of the intended environment, which consists of
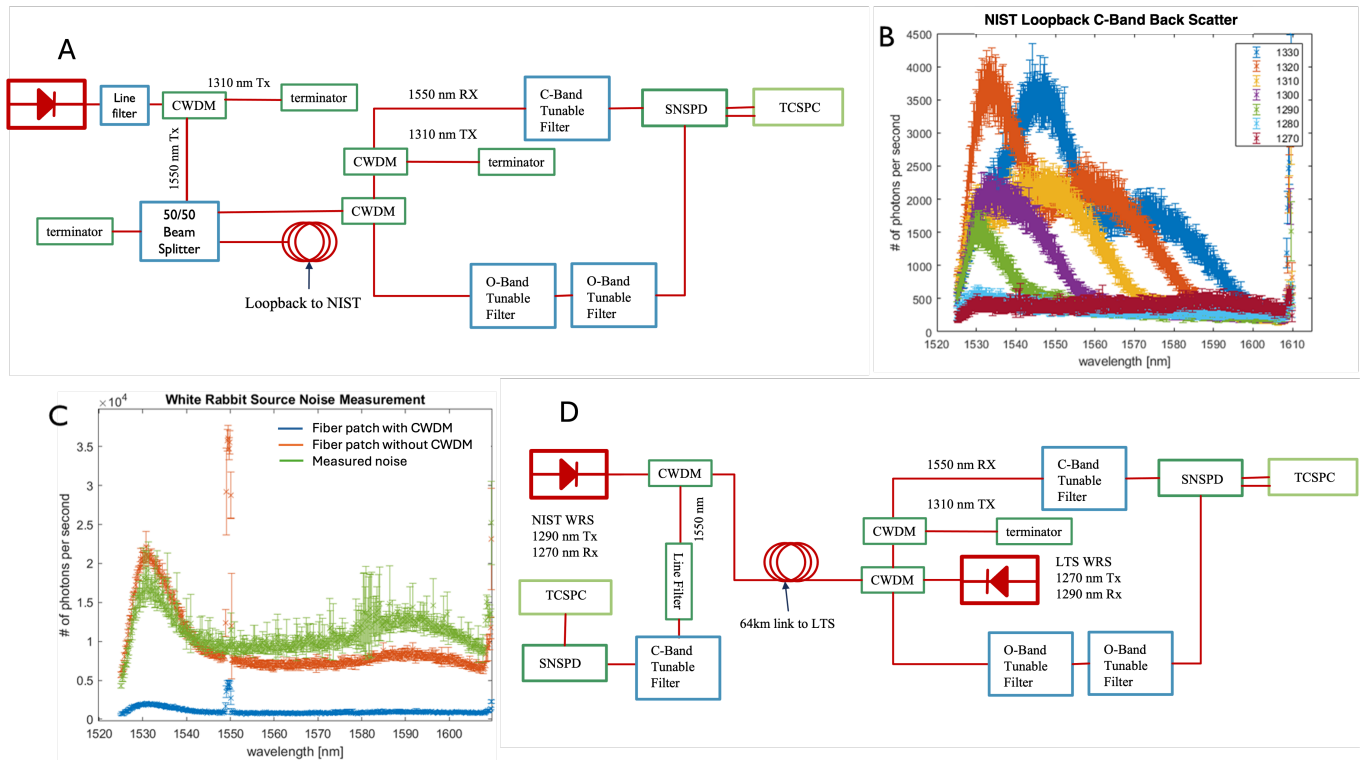
FIG. 18. (A-B) The experimental setup and measurements for a clean laser source in the O-Band over the 128 km loopback fiber from LTS to UMD to NIST. We used a Santec TSL-570 O-band tunable laser to inject 1 mW light. Each wavelength was measured 20 times, and the results averaged with the standard deviation represented as the error bars. (C) shows the measured noise over the 128 km loopback from the tunable laser in green and the SFPs measured directly with only a fiber patch in orange. The two curves are comparable, indicating that most of the noise is due to the source and not scattering in the fiber. The blue shows the measurement of the SFP with a fiber patch and a CWDM filter This graph shows nearly an order of magnitude improvement in the baseline noise level with filtered sources. The measurements show a peak near 1550 nm that is not in the data measured over the deployed fiber with a clean source. We believe the peak is due to back scatter from the 1270 nm SFP.

crosstalk between fibers, patch panels, and switches. In the case of co-existing quantum and classical signals on the same fiber, the main source of noise is expected to be light scattered from the classical signal[45]. While most of the scattering will be Rayleigh, the main concern in the single-photon regime is broad stimulated Raman scattering, as the Brillioun scattering is within the same DWDM channel, which will affect the entire band, forcing the choice of a quantum source to be detuned from the classical source in a separate, higher loss band. The asymmetry of the Raman scattering leads to an advantage to have the quantum signal on the anti-stokes side of the classical signal, which can be up to 3 orders of magnitude weaker than the Stokes[46]. However, to mitigate loss, it is more desirable to have the quantum signal in the C-Band, and the classical signal in the O-Band, sufficiently detuned in wavelength to avoid interference from the Raman Stokes peak[9]. Prior laboratory and campus scale measurements indicated that WR-PTP can co-exist with quantum networking protocols such as entanglement distribution[10].

To assess the viability of co-existence over the deployed links, the noise profile must be characterized at the single photon level. Scattered light from the fiber was measured with tunable filters (Santec) scanning with a bin width of 0.8 nm

(roughly the width of a DWDM channel) with a step size of 25 GHz. The set up (Fig.18) was modified to reduce the light leakage from the filters, showing counts comparable to detector dark counts. Both the C and O Bands showed a flat response to the change in wavelength; however, before the terminators and CWDM were added, specific features in the O band that matched the literature were recorded[45]. The elimination of these features with added isolation of the source implies they were the result of light instabilities from the source rather than a scattering effect. Similar results were found when measuring the WR-PTP source directly, emphasizing the need to isolate the noise produced directly from the source before coupling the quantum signal. Our results measured over the deployed link show that for a clean source transmitting a 1 mW classical signal in the O-Band, a quantum source signal can co-propagate in the C-Band using the same link. For an O-Band source 1280 nm and below, a quantum signal at 1550 nm would experience negligible additional noise from the classical source (Fig.18). We deployed the 1270 nm and 1290 nm CWDM SFPs over 64 km duplex fibers between NIST and LTS, with sub-10 ps TDEV from 1 s to 10^4 s averaging periods. However, the SFPs will require additional filtering in order to co-propagate a quantum signal over the

deployed link.

V. DISCUSSION

A. Capabilities and Limitations

We have described the design and characterization of one of the first readily scalable synchronization network based on atomic clocks specifically to meet quantum networking research requirements and to understand the needed areas for improvement in a metropolitan-scale testbed. The TDEV of the fiber-based optical time transfer stability generally ranged from 10^{-12} at short time intervals for both solutions with and without active phase stabilization. With active phase stabilization, we show two DC-QNet links can maintain 10^{-12} with one month averaging periods. Path delay gradients, strongly correlated with air temperature gradients, remains the dominant source of clock transfer instabilities among the remote nodes. Additional characterization was also necessary to understand and compensate for errors from chromatic dispersion, polarization drift, polarization-dependent loss, and optical power fluctuations to meet the picosecond-level error budget. While underground fibers can significantly mitigate the fluctuations induced by air temperature changes, it is also important for the future resilience and scalability of quantum networks to be able to manage and compensate for the phase noise for both time and quantum information transfer. Furthermore, improvements to enable flexibility in the co-propagation of quantum and classical signals by effectively filtering or managing noisy environments will be needed. To that end, we are exploring network probe measurements at the single photon level or using parallel fibers as well as algorithmic methods to manage environmental dynamics.

B. WR Improvement Opportunities

To increase the WRS synchronization precision towards the sub-10 ps needed for quantum network measurements, we have gathered information on various parameters that affect synchronization and plan to build models that will predict the required corrections. Such parameters include environmental information such as ambient outside temperature for aerial fibers, SFP temperature, and SFP Tx and Rx optical power that we can sample in real-time. We are pursuing more precise delay information using single-photon measurements such as quantum optical time domain reflectometry. From these models and measurements, we plan to get real-time delay corrections for the WRS in the form of picosecond-level correction values that we believe can be additively combined into a single value. We believe that we can affect that correction in the WRS via dynamic updates to the alpha coefficient, which accounts for the path delay asymmetry. The alpha coefficient was originally used to correct wavelength asymmetry due to chromatic dispersion[47] and was a static, calibrated value. A recent enhancement[48] made to the WRS software allows real-time asymmetry coefficient updates. Adjusting the asymmetry coefficient will have the effect of dynamically updating the WRS delay calculation, resulting in a correction to the phase delay of the 1 PPS, 10 MHz, and 62.5 MHz clocks, yielding more precise time synchronization of instrumentation used in quantum networking experiments.

VI. CONCLUSION

DC-QNet has established and characterized two methods of time synchronization to enable the development of near-term quantum networking protocols. We observed picosecond level TDEV between 1 s to over months of observations with active phase compensation, where the time stability is limited by the stability of the reference clock. With WR-PTP, the synchronization network shows sub-10 ps TDEV at 1-day observation intervals. For picosecond-level or better phase stabilization and polarization compensation, co-propagating probe signals at single-photon scales will likely be beneficial. The bright light from the time synchronization signal requires filtering to reduce light leakage and limits the quantum channel coexistence to a separate band. Given the availability of highly stable reference clocks and the characterized time transfer capabilities of DC-QNet, our future work will continue to advance single photon network probes and explore machine learning algorithms to measure, predict, and compensate for the link instabilities. The capabilities can be further improved and extended to meet the security requirements, which can potentially be best met by developing quantum time synchronization[18,49] based on highly stable time transfer between a network of atomic clocks that remains resilient and secure in the presence of environmental noise in the fiber links.

VII. REFERENCES

[1] J. S. Bell, "On the einstein podolsky rosen paradox," Physics Physique Fizika **1**, 195 (1964).

[2] J. I. Cirac, P. Zoller, H. J. Kimble, and H. Mabuchi, "Quantum state transfer and entanglement distribution among distant nodes in a quantum network," Phys. Rev. Lett. **78**, 3221–3224 (1997).

[3] J. F. Dynes, H. Takesue, Z. L. Yuan, A. W. Sharpe, K. Harada, T. Honjo, H. Kamada, O. Tadanaga, Y. Nishida, M. Asobe, and A. J. Shields, "Efficient entanglement distribution over 200 kilometers," Opt. Express **17**, 11440–11449 (2009).

[4] J. Yin, Y. Cao, Y.-H. Li, S.-K. Liao, L. Zhang, J.-G. Ren, W.-Q. Cai, W.-Y. Liu, B. Li, H. Dai, G.-B. Li, Q.-M. Lu, Y.-H. Gong, Y. Xu, S.-L. Li, F.-Z. Li, Y.-Y. Yin, Z.-Q. Jiang, M. Li, J.-J. Jia, G. Ren, D. He, Y.-L. Zhou, X.-X. Zhang, N. Wang, X. Chang, Z.-C. Zhu, N.-L. Liu, Y.-A. Chen, C.-Y. Lu, R. Shu, C.-Z. Peng, J.-Y. Wang, and J.-W. Pan, "Satellite-based entanglement distribution over 1200 kilometers," Science **356**, 1140–1144 (2017), https://www.science.org/doi/pdf/10.1126/science.aan3211.

[5] J.-W. Pan, D. Bouwmeester, H. Weinfurter, and A. Zeilinger, "Experimental entanglement swapping: entangling photons that never interacted," Physical review letters **80**, 3891 (1998).

[6] R. Kaltenbaek, R. Prevedel, M. Aspelmeyer, and A. Zeilinger, "High-fidelity entanglement swapping with fully independent sources," Physical Review A **79**, 040302 (2009).

[7] F. Samara, N. Maring, A. Martin, A. S. Raja, T. J. Kippenberg, H. Zbinden, and R. Thew, "Entanglement swapping between independent and asyn-

chronous integrated photon-pair sources," Quantum Science and Technology **6**, 045024 (2021).

[8] T. Gerrits *et al.*, "White rabbit-assisted quantum network node synchronization with quantum channel coexistence," Conference on Lasers and Electro-Optics (2022).

[9] I. A. Burenkov *et al.*, "Synchronization and coexistence in quantum networks," Opt. Express **31**, 11431–11446 (2023).

[10] A. Rahmouni, P. Kuo, Y. Li-Baboud, I. Burenkov, Y. Shi, M. Jabir, N. Lal, D. Reddy, M. Merzouki, L. Ma, *et al.*, "Metropolitan-scale entanglement distribution with co existing quantum and classical signals in a single fiber," arXiv preprint arXiv:2402.00617 (2024).

[11] J. M. Thomas, F. I. Yeh, J. H. Chen, J. J. Mambretti, S. J. Kohlert, G. S. Kanter, and P. Kumar, "Quantum teleportation coexisting with conventional classical communications in optical fiber," arXiv preprint arXiv:2404.10738 (2024).

[12] M. Alshowkan, P. G. Evans, B. P. Williams, N. S. V. Rao, C. E. Marvinney, Y.-Y. Pai, B. J. Lawrie, N. A. Peters, and J. M. Lukens, "Advanced architectures for high-performance quantum networking," J. Opt. Commun. Netw. **14**, 493–499 (2022).

[13] N. Lal, I. A. Burenkov, Y.-S. Li-Baboud, M. V. Jabir, P. S. Kuo, T. Gerrits, O. Slattery, and S. V. Polyakov, "Synchronized source of indistinguishable photons for quantum networks," Opt. Express **32**, 18257–18267 (2024).

[14] C. H. Bennett and G. Brassard, "Quantum cryptography: Public key distribution and coin tossing," Theoretical Computer Science **560**, 7–11 (2014), theoretical Aspects of Quantum Cryptography – celebrating 30 years of BB84.

[15] C. L. Degen, F. Reinhard, and P. Cappellaro, "Quantum sensing," Reviews of modern physics **89**, 035002 (2017).

[16] R. Van Meter and S. J. Devitt, "The path to scalable distributed quantum computing," Computer **49**, 31–42 (2016).

[17] P. Kómár, E. M. Kessler, M. Bishof, L. Jiang, A. S. Sørensen, J. Ye, and M. D. Lukin, "A quantum network of clocks," Nature Physics **10**, 582–587 (2014).

[18] C. Spiess, S. Töpfer, S. Sharma, A. Kržič, M. Cabrejo-Ponce, U. Chandrashekara, N. L. Döll, D. Rieländer, and F. Steinlechner, "Clock synchronization with correlated photons," Physical Review Applied **19**, 054082 (2023).

[19] T.-Y. Chen, X. Jiang, S.-B. Tang, L. Zhou, X. Yuan, H. Zhou, J. Wang, Y. Liu, L.-K. Chen, W.-Y. Liu, *et al.*, "Implementation of a 46-node quantum metropolitan area network," npj Quantum Information **7**, 134 (2021).

[20] M. Alshowkan *et al.*, "Reconfigurable quantum local area network over deployed fiber," PRX Quantum **2**, 040304 (2021).

[21] L. Castillo-Veneros, D. Du, G. Cui, D. Cottrill, P. Stankus, D. Katramatos, J. Martínez-Rincón, M. Flament, M. Namazi, and E. Figueroa, "Developing a layered quantum-capable internet," in *Quantum 2.0 Conference and Exhibition* (Optica Publishing Group, 2022) p. QW4A.1.

[22] J. Chung, E. M. Eastman, G. S. Kanter, K. Kapoor, N. Lauk, C. H. Pena, R. K. Plunkett, N. Sinclair, J. M. Thomas, R. Valivarthi, *et al.*, "Design and implementation of the illinois express quantum metropolitan area network," IEEE Transactions on Quantum Engineering **3**, 1–20 (2022).

[23] E. Bersin, M. Grein, M. Sutula, R. Murphy, Y. Q. Huan, M. Stevens, A. Suleymanzade, C. Lee, R. Riedinger, D. J. Starling, *et al.*, "Development of a boston-area 50-km fiber quantum network testbed," Physical Review Applied **21**, 014024 (2024).

[24] H. Buhrman, N. Chandran, S. Fehr, R. Gelles, V. Goyal, R. Ostrovsky, and C. Schaffner, "Position-based quantum cryptography: Impossibility and constructions," SIAM Journal on Computing **43**, 150–178 (2014).

[25] A. Bluhm, M. Christandl, and F. Speelman, "A single-qubit position verification protocol that is secure against multi-qubit attacks," Nature Physics **18**, 623–626 (2022).

[26] L. Escolà-Farràs and F. Speelman, "Single-qubit loss-tolerant quantum position verification protocol secure against entangled attackers," Physical Review Letters **131**, 140802 (2023).

[27] S. R. Jefferts, M. A. Weiss, J. Levine, S. Dilla, E. W. Bell, and T. E. Parker, "Two-way time and frequency transfer using optical fibers," IEEE transactions on instrumentation and measurement **46**, 209–211 (1997).

[28] J. Ye, J.-L. Peng, R. J. Jones, K. W. Holman, J. L. Hall, D. J. Jones, S. A. Diddams, J. Kitching, S. Bize, J. C. Bergquist, L. W. Hollberg, L. Robertsson, and L.-S. Ma, "Delivery of high-stability optical and microwave frequency standards over an optical fiber network," J. Opt. Soc. Am. B **20**, 1459–1467 (2003).

[29] I. Coddington, W. C. Swann, L. Lorini, J. C. Bergquist, Y. Le Coq, C. W. Oates, Q. Quraishi, K. Feder, J. Nicholson, P. S. Westbrook, *et al.*, "Coherent optical link over hundreds of metres and hundreds of terahertz with subfemtosecond timing jitter," Nature Photonics **1**, 283–287 (2007).

[30] S. M. Foreman, K. W. Holman, D. D. Hudson, D. J. Jones, and J. Ye, "Remote transfer of ultrastable frequency references via fiber networks," Review of Scientific Instruments **78** (2007).

[31] P. Koppang, J. Skinner, and D. Johns, "Usno master clock design enhancements," in *Proceedings of the 38th Annual Precise Time and Time Interval Systems and Applications Meeting* (2006) pp. 185–192.

[32] S. Peil, T. B. Swanson, J. Hanssen, and J. Taylor, "Microwave-clock timescale with instability on order of 1017," Metrologia **54**, 247 (2017).

[33] "Ieee standard for a precision clock synchronization protocol for networked measurement and control systems," IEEE Std 1588-2008 (Revision of IEEE Std 1588-2002) , 1–269 (2008).

[34] T. Lodhen, D. Cottrill, L. Castillo-Veneros, J. Martínez-Rincón, D. Katramatos, P. Stankus, and E. Figueroa, "Towards distribution of memory-compatible polarization entanglement over long distances," in *Quantum 2.0* (Optica Publishing Group, 2023) pp. QTh2A–40.

[35] W. McKenzie, Y.-S. Li-Baboud, *et al.*, "Towards quantum networking: Characterization of white rabbit precision time protocol over a metropolitan scale fiber link," in *Precise Time and Time Interval Meeting*, Session P3b (ION, Long Beach, CA, 2024).

[36] J. Serrano, M. Lipinski, T. Wlostowski, E. Gousiou, E. van der Bij, M. Cattin, and G. Daniluk, The White Rabbit Project (2013).

[37] Certain commercial equipment, instruments, or materials are identified in this paper to foster understanding. Such identification does not imply recommendation or endorsement by the National Institute of Standards and Technology, the Department of Defense, or the National Aeronautics and Space Administration, nor does it imply that the materials or equipment identified are necessarily the best available for the purpose.

[38] P. Krehlik, Ł. Śliwczyński, Ł. Buczek, J. Kołodziej, and M. Lipiński, "Elstab—fiber-optic time and frequency distribution technology: A general characterization and fundamental limits," IEEE transactions on ultrasonics, ferroelectrics, and frequency control **63**, 993–1004 (2015).

[39] J. L. Hanssen, J. A. Taylor, and C. R. Ekstrom, "Time and frequency transfer over an electronically compensated fiber link," (2013) pp. 235–238.

[40] M. L. O. Lopez, A. Amy-Klein, "High-resolution microwave frequency dissemination on an 86-km urban optical link," Appl. Phys. B **98**, 723–727 (2010).

[41] S. Droste, F. Ozimek, T. Udem, K. Predehl, T. W. Hänsch, H. Schnatz, G. Grosche, and R. Holzwarth, "Optical-frequency transfer over a single-span 1840 km fiber link," Phys. Rev. Lett. **111**, 110801 (2013).

[42] M. Rost, D. Piester, W. Yang, T. Feldmann, T. Wübbena, and A. Bauch, "Time transfer through optical fibres over a distance of 73 km with an uncertainty below 100 ps," Metrologia **49**, 772 (2012).

[43] Open Weather API, Https://openweathermap.org/current.

[44] L. C. Sinclair, F. R. Giorgetta, W. C. Swann, E. Baumann, I. Coddington, and N. R. Newbury, "Optical phase noise from atmospheric fluctuations and its impact on optical time-frequency transfer," Physical Review A **89**, 023805 (2014).

[45] J. M. Thomas, G. S. Kanter, and P. Kumar, "Designing noise-robust quantum networks coexisting in the classical fiber infrastructure," Optics Express **31**, 43035–43047 (2023).

[46] J.-Q. Geng, G.-J. Fan-Yuan, S. Wang, Q.-F. Zhang, Y.-Y. Hu, W. Chen, Z.-Q. Yin, D.-Y. He, G.-C. Guo, and Z.-F. Han, "Coexistence of quantum key distribution and optical transport network based on standard single-mode fiber at high launch power," Optics Letters **46**, 2573–2576 (2021).

[47] P. Jansweijer and H. Peek, "In-situ determination of the fiber delay coefficient in time-dissemination networks," in *2019 IEEE International Symposium on Precision Clock Synchronization for Measurement, Control, and Communication (ISPCS)* (2019) pp. 1–6.

[48] Wujek, Adam, Alpha Adjustment Code,https://ohwr.org/project/ppsi/tree/adam-alpha_adjustment.

[49] E. S. Polzik and J. Ye, "Entanglement and spin squeezing in a network of distant optical lattice clocks," Physical Review A **93**, 021404 (2016).